Available online at www.sciencedirect.com
SCIENCE DIRECT
Polymer 47 (2006) 6140–6148
polymer
www.elsevier.com/locate/polymer

Supramolecular assembled C_{60}-containing carboxylated poly(dimethylsiloxane) composites

Jianying Ouyang [a], Yi Pan [a], Shuiqin Zhou [a,*], Suat Hong Goh [b]

[a] *Department of Chemistry, College of Staten Island and The Graduate Center, City University of New York, 2800 Victory Blvd, Staten Island, NY 10314, United States*

[b] *Department of Chemistry, National University of Singapore, Singapore 117543, Singapore*

Received 24 March 2006; received in revised form 6 June 2006; accepted 9 June 2006
Available online 11 July 2006

Abstract

Supramolecular assembled nanocomposites were prepared through the solution casting of the complexing mixtures from the side chain carboxylated poly(dimethylsiloxane) (PDMS) with the 1-(4-methyl)-piperazinylfullerene (MPF). FT-IR and XPS analyses reveal that there are strong ionic interactions between the two components. Small-angle X-ray scattering study shows the formation of MPF fullerene nanodomains dispersed in the PDMS matrix, but no highly ordered structures, which is confirmed with TEM images. Compared to its polymeric precursor, the MPF crosslinked composites exhibit superior thermal mechanical stability and dramatic increase in the storage and loss moduli. Moreover, elastic response exceeds viscous response in the composites due to the formation of crosslinking structures. The increase of the MPF content in the composites leads to a denser packing of MPF nanodomains, resulting in better thermal, mechanical, and viscoelastic properties. The decrease in the carboxylic acid groups along the PDMS chains reduces the crosslinking density of the PDMS/MPF composites. The composites show a combined dielectric property from both PDMS and MPF components.

Keywords: C_{60} fullerene; Poly(dimethylsiloxane); Supramolecular assembled composites

1. Introduction

One of the efficient ways to improve the processibility of C_{60} is by introducing it into polymers to take advantage of the excellent processibility of polymers such as good film-forming ability, tunable compositions and conformations. C_{60}-fullerene based polymeric materials have received great attention in recent years [1–9]. Among the various methods to attach C_{60} onto polymers [10–20], it is simpler and more convenient to embed C_{60} physically in polymer matrixes. Functionalization of C_{60} and/or polymers is often carried out to improve the compatibility of C_{60} with polymers.

Recently, we have successfully prepared supramolecular assembled C_{60}-containing polymeric materials based on the interactions between the functionalized C_{60} and polymers possessing suitable functional groups [21–24]. The C_{60} was either mono-functionalized or multi-functionalized, and the interactions between complementary functional groups of C_{60} derivatives and polymers enable the C_{60} derivatives to be well dispersed and adhere strongly to the polymer matrixes, leading to a significant improvement on the storage moduli of the materials. While the interactions between C_{60} species and polymers were mainly hydrogen-bonding or ionic interaction, the hydrophobic interactions could also play a vital role to control the morphology and properties of the resulted C_{60}-polymer composites [24]. For example, a three-dimensional network structure could be constructed through the hydrogen-bonding interaction between the hydroxyl groups in fullerenol and the terminal amine groups of polydimethylsiloxane (PDMS) chains. The strong hydrophobic interactions among C_{60} molecules render the formation of C_{60} nanodomains, which could be homogeneously confined in the

* Corresponding author. Tel.: +1 718 982 3897; fax: +1 718 982 3910.
E-mail address: zhoush@mail.csi.cuny.edu (S. Zhou).

0032-3861/$ - see front matter © 2006 Elsevier Ltd. All rights reserved.
doi:10.1016/j.polymer.2006.06.026

polymer matrix. This unique structure of the fullerenol–PDMS nanocomposites leads to excellent film-forming ability, superior thermal and mechanical stability, and advantageous dielectric property, i.e. increased permittivity and greatly decreased loss factor at a high content of polyhydroxylated fullerenol [24].

In the present work, we design side chain functionalized polymers to interact with the multifunctional 1-(4-methyl)-piperazinylfullerene (MPF) to form a novel structured C_{60}-polymer composite material. It has been indicated that MPF can form complexes with the proton-donating polymers such as poly(styrene-sulfonic acid), poly(vinylphosphonic acid), poly(acrylic acid) and poly(methacrylic acid) through ionic interactions [25]. On the other hand, PDMS polymer has many excellent properties such as low glass transition temperature, very low surface energy, low gas permeability, good thermal stability, and biocompatibility [26,27]. Furthermore, PDMS can be modified to attach carboxylic groups on the side chains and the content of carboxylic groups is tunable [27]. It was envisaged that there would be strong ionic interactions between the amine groups of MPF and the side carboxylic acid groups on the PDMS chains to achieve good dispersion and tight affinity of C_{60} in the PDMS matrix so that the outstanding properties of both C_{60} and PDMS materials can be combined. The interactions between the MPF and the side chain carboxylated PDMS chains, the ordered structures of the resulted C_{60}-PDMS composites as well as their thermal, thermal mechanical, viscoelastic, and dielectric properties were investigated in this paper. The effects of the MPF contents and the carboxylic acid group density of PDMS chains on the properties of the PDMS/MPF composites were discussed.

2. Experimental

2.1. Materials and composites preparation

[60]Fullerene (C_{60}) (99.5%) was purchased from SES research company, USA. 1-Methylpiperazine (98%), (3-cyanopropyl)methyldichlorosilane and dichlorodimethylsilane were supplied by Sigma–Aldrich Company. Both chlorobenzene and tetrahydrofuran of AR grade were obtained from Fisher Scientific Company. 1-(4-Methyl)-piperazinylfullerene (MPF) in brown powders was synthesized and characterized according to Ref. [25], which has an average stoichiometry of $[C_{60}H_9(NC_4H_8NCH_3)_9]$ as determined by X-ray photoelectron spectroscopy.

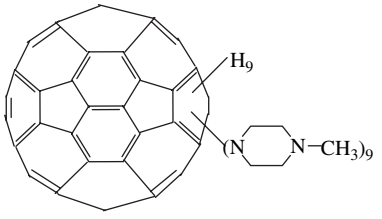

MPF

Two random copolymers of dimethylsiloxane and (3-carboxypropyl)methylsiloxane with 45.4 mol % and 25.2 mol % of (3-carboxypropyl)methylsiloxane unit were synthesized and characterized according to the reported method [28]. The content of (3-carboxypropyl)methylsiloxane unit was determined by ^{1}H NMR. These transparent and gel-like copolymers are denoted as PSI45 and PSI25, where the number after PSI denotes the molar percentage of (3-carboxypropyl)methylsiloxane unit. Their molecular weights were estimated by gel permeation chromatography with THF as eluent (1.0 ml/min) and polystyrene as standards, which are 3.2×10^4 g/mol for PSI45 and 4.1×10^4 g/mol for PSI25, respectively, with polydispersity of about 1.7 for both polymers.

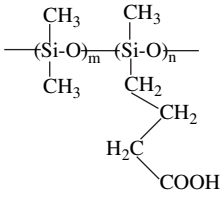

PSIX

To prepare PSIXMPF composites, an appropriate amount of MPF suspension in THF after being sonicated for half an hour was added into the THF solution of PSIX. The PSIX concentration in the mixture was kept at 9.2 mg/ml. The mixture was continuously stirred overnight followed by evaporation at room temperature. Five composites were prepared for PSI45MPF system, denoted as PSI45MPF15, PSI45MPF36, PSI45MPF56, PSI45MPF74, and PSI45MPF116, corresponding to an increase in the content of MPF with the molar ratio of N/COOH (mol %) at 15, 36, 56, 74, and 116, respectively (the weight percentage of MPF in the above composites is 5.2, 11.5, 17.1, 21.4 and 27.0%, accordingly). Similarly, five composites were prepared for PSI25MPF system, denoted as PSI25MPF14, PSI25MPF33, PSI25MPF53, PSI25MPF72, and PSI25MPF106, corresponding to an increase in the content of MPF with the molar ratio of N/COOH (mol %) at 14, 33, 53, 72, and 106, respectively (the weight percentage of MPF in the above composites is 3.2, 7.1, 11.7, 15.0 and 20.2%, accordingly). The samples were finally dried in vacuo at 50 °C for three days to afford films.

2.2. FT-IR characterization

The infrared spectra were recorded on a Nicolet Magna 550 FT-IR spectrometer. The spectra were signal-averaged from 16 scans with a resolution of 4 cm^{-1}. The THF solutions of PSIX were sprayed on PTFE film, and the composites were ground with KBr followed by being compressed into pellets. All sample pellets were dried in vacuo at 60 °C for 2 h just before measurement to exclude moisture.

2.3. XPS analysis

X-ray photoelectron spectroscopy (XPS) measurements were made on a VG ESCALAB MKII spectrometer with an Mg Kα X-ray source (1253.6 eV photons) and a hemispherical energy analyzer. Samples were mounted on studs using a double-sided adhesive tape. The X-ray source was run at

12 kV and 10 mA. A pass energy of 20 eV and a rate of 0.05 eV/step were used for all XPS spectra acquisitions with a binding energy width of 12 eV. The pressure in the analysis chamber was maintained at 10^{-8} mbar or lower during the measurements. All spectra were obtained at a take-off angle of 75° and they were curve-fitted with XPSPEAK3.1. To compensate the surface charging effects, all binding energies were referenced to the saturated hydrocarbon C1s peak at 285.0 eV.

2.4. Small-angle X-ray scattering (SAXS) measurements

SAXS measurements were performed at the Advanced Polymers-PRT Beamline (X27C), National Synchrotron Light Source (NSLS) at Brookhaven National Laboratory (BNL), using a laser-aided prealigned pinhole collimator. The incident beam wavelength (λ) was tuned at 0.1366 nm. A two-dimensional imaging plate was used in conjunction with an image scanner as the detection system. The sample to detector distance for SAXS was 795 mm. The scattering vector q is expressed as $q = (4\pi/\lambda)\sin(\theta/2)$ with θ being the scattering angle between the incident and the scattered X-rays. The d-spacing of the ordered structures can be calculated as $d = 2\pi/q$.

2.5. Thermal analyses

The measurement of glass transition temperatures (T_gs) was made with a TA Instruments Q100 differential scanning calorimeter (DSC) under a flow of 50 ml min^{-1} purified nitrogen at a heating rate of 20 °C min^{-1}. The abrupt increase of heat capacity in the DSC trace was taken as T_g. Thermal stability was analyzed under a flow of 60 ml min^{-1} purified nitrogen at a heating rate of 10 °C min^{-1} using a Hi-Res TGA 2950 thermogravimetric analyzer, TA Instruments. Thermal mechanical analyses (TMA) were performed in compression mode with a flat-tipped standard expansion probe using a TA instruments TMAQ400 under a flow of 50 ml min^{-1} purified nitrogen. Samples were cooled in situ to −130 °C or −150 °C with liquid nitrogen, then heated up at a rate of 5 °C min^{-1}.

2.6. Rheometry

Viscoelastic behaviors of various samples were investigated using a shear strain-controlled rheometer (ARES RFS rheometer, TA Instruments) with 25 mm parallel plates. The temperature ramp measurements were carried out from −20 °C to 120 °C at 1 Hz. The strain was 10% for PSI45 and PSI45MPF15, and 1% for PSI45MPF36 and PSI45MPF56. The temperature was controlled by the peltier assembly with an accuracy of 0.01 °C. Both storage and loss moduli were measured from linear viscoelastic spectra.

2.7. Dielectric analyses

The dielectric analysis was carried out on a TA Instruments Dielectric Analyzer 2970, covering a frequency range from 1 Hz to 100 kHz and a temperature range from −120 °C to 100 °C. The dielectric spectra were obtained in single surface mode except for MPF in ceramic parallel plate mode at a heating rate of 3 °C min^{-1} in purified nitrogen.

3. Results and discussion

3.1. Interaction between MPF and PSIX

Fig. 1a shows the carbonyl-stretching region of PSI45 compared with that of PSI45MPF composites. The carbonyl stretch of PSI45 has a main band centered at 1711 cm^{-1} as well as a shoulder band at 1739 cm^{-1}. The 1711 cm^{-1} band is assigned to the carbonyl groups in self-associated carboxylic groups (acid dimers), and the 1739 cm^{-1} band belongs to the free carbonyl groups without association. These characteristic peaks of carboxylic groups are commonly observed

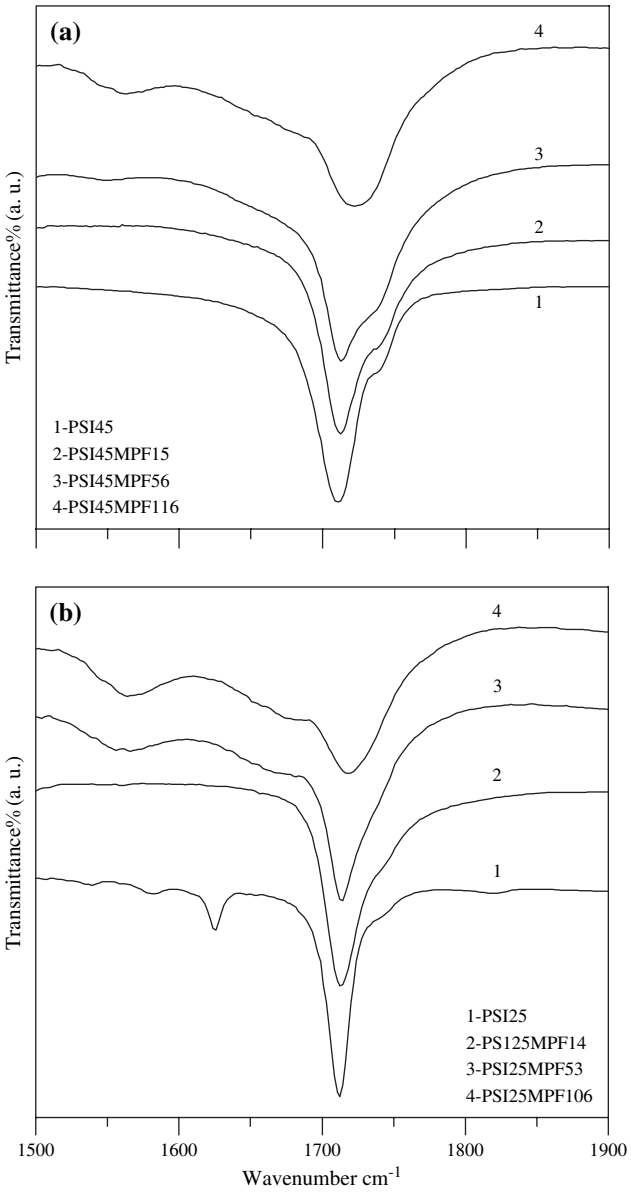

Fig. 1. FT-IR spectra of the carbonyl region of (a) PSI45 and PSI45MPF composites, and (b) PSI25 and PSI25MPF composites, respectively.

in FT-IR spectra of other carboxylated polymers, such as poly(acrylic acid) (PAA) and poly(methacrylic acid) (PMAA), and PSI100 [28,29]. The free carboxylic band at 1739 cm^{-1} is more distinctive in PSI45 than that in fully carboxylated PAA, PMAA and PSI100, which are disguised in a broad band centered at 1710 cm^{-1}. After PSI45 was complexed with MPF, the free carbonyl-stretching band grows in intensity at the expense of the acid dimers. It is known that the self-association of the acidic groups must be broken up before new intermolecular interactions are formed, which is particularly evident with carboxylic acid containing polymers [30]. With the increase in the content of MPF in the composites, the dimeric band is gradually shifted to a higher frequency. Eventually, the carbonyl-stretching band is reshaped into a single band centered at 1724 cm^{-1} in composite PSI45MPF116, which means that all carboxylic groups of PSI45 are reorganized due to the interaction with amine groups of MPF and there are no unaffected acid dimers existed. Meanwhile, a clear band at 1562 cm^{-1} from the asymmetric stretching mode of COO^- appeared, indicating an ionic interaction formed between PSI45 and MPF.

Similar changes of carbonyl-stretching region are observed in PSI25MPF composites as shown in Fig. 1b. The small band at 1623 cm^{-1} might be originated from impurities in PSI25. With the increase in the MPF content in the composites, the intensity of free carbonyl-stretching band increases and the intensity of dimeric band relatively decreases and shifted to higher frequency. Finally, the carbonyl-stretching band in composite PSI25MPF106 is totally reshaped into a single band centered at 1719 cm^{-1} and the COO^- band at 1563 cm^{-1} is clearly observed, indicating the dominant ionic interactions between MPF and PSI25.

The interactions between the tertiary amine groups of MPF and the carboxylic groups of PSI45 are also evident from XPS studies, as shown in Fig. 2. The N1s spectrum of MPF shows a symmetrical peak centered at a binding energy (BE) of 399.0 eV. The N1s peak is narrow (FWHM = 1.55 eV), so no deconvolution was carried out for this peak. In contrast, the N1s peak of composite PSI45MPF116 can be curve-fitted by two component peaks, with one remaining at 399.0 eV and the other at 401.3 eV. The appearance of the new high-BE energy peak clearly shows that some of the amine groups of MPF interact with the carboxylic acid groups in PSI45. Our previous studies have shown that when the nitrogen of pyridine, piperidine or imidazole is protonated, the BE value of N1s is increased by 2.0 eV or more, whereas hydrogen-bonding interaction will increase the BE value by about 1.0 eV [31–35]. The increase in the binding energy of N1s of MPF by 2.3 eV indicated that the interaction between MPF and PSI45 is of ionic nature. The protonated nitrogen atoms are up to 51% according to the fraction of area. Lu and others carefully characterized the interactions between MPF and acidic polymers using XPS [25], which demonstrated that the nitrogen atoms in MPF are readily protonated and the nitrogen far away from C_{60} (nitrogen B) is the much more preferred site of protonation than that near the cage of C_{60} (nitrogen A). Similarly, it is most likely that the majority

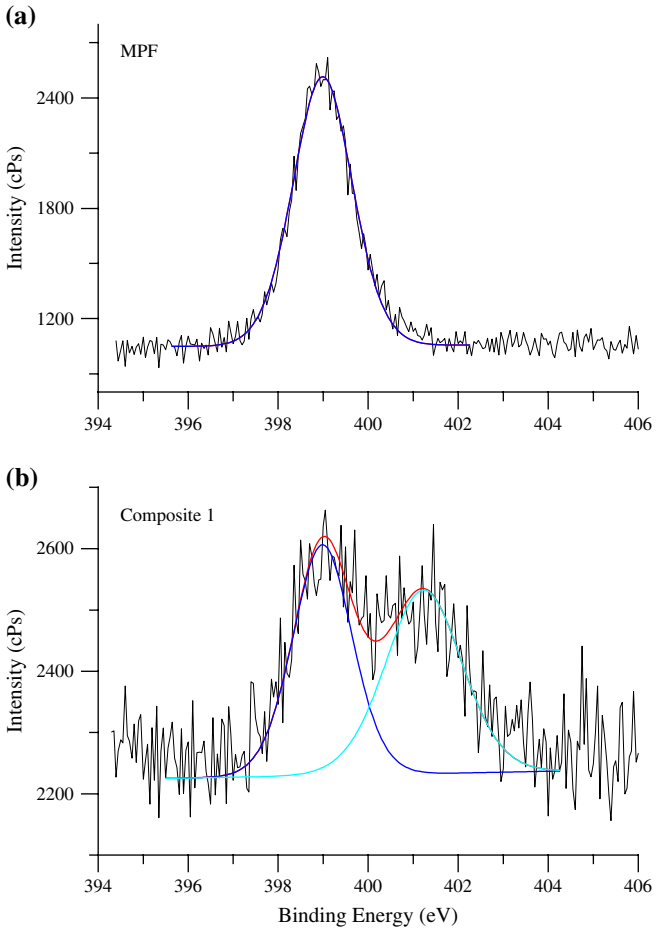

Fig. 2. XPS N1s spectra of (a) MPF and (b) PSI45MPF116 composites.

of protonation occurs at the nitrogen B in the PSIXMPF composites. It is also noted that the N1s peak at 401.3 eV is broader than the one at 399.0 eV, which indicates that the chemical environments are more complicated for those nitrogen atoms with higher binding energies. One probable reason could be that the binding energy difference between the two types of nitrogen atoms is increased when one type of amine groups (likely nitrogen B) directly interacts with −COOH, which induces the change of chemical environment of another type of amine groups (nitrogen A). Although no effort was made in this paper to deconvolute the two types of nitrogen, the BE of nitrogen A is 0.4 eV higher than that of nitrogen B in MPF [25].

3.2. Structures of PSIX/MPF complexes

Fig. 3 shows the SAXS profiles of the PSI45 polymer and the dried PSI45MPF composites formed at different content of MPF. While the PSI45 polymer had no scattering peaks in the experimental q range, the complexation of MPF to the PDMS matrix produced a single scattering peak, implicating the homogeneous distributions of the MPF domains in the PDMS matrix but no highly ordered close packing structure. The increase of MPF in the composites from 5.2 wt%

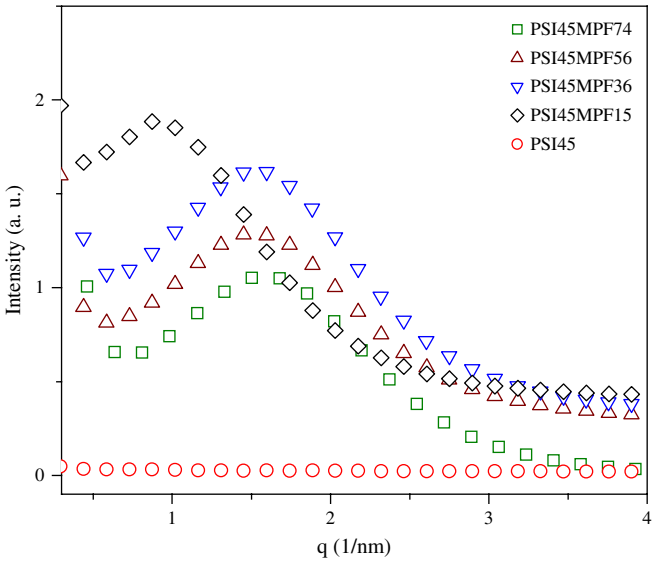

Fig. 3. SAXS profiles of PSI45MPF composites.

(PSI45MPF15) to 11.5 wt% (PSI45MPF36) shifted the peak position to higher q_{max} values significantly, corresponding to a gradual decrease in the inter-distances of MPF nanodomains. However, the further increase of MPF content from 11.5 wt% to 21.4 wt% only shifted the q_{max} position slightly. This result could be attributed to the saturation of the binding sites along the PDMS chains, in which all the COOH functional groups were complexed with the MPF nanodomains when MPF content was above a certain value. After this saturation, the continuous addition of MPF will be used to increase the individual MPF nanodomain size, which will actually increase the inter-distance of MPF nanodomains slightly. Thus, it is possible to observe a nearly constant q_{max} position when MPF content is in a certain high range. Interestingly, this structure is totally different from the structure of composites formed by multifunctional fullerenes with terminal functionalized PDMS [24], where the increase in the multifunctional fullerene content increases the inter-distances of fullerene nanodomains continuously. When the terminal functionalized PDMS chains are used to complex with fullerene derivatives, the distance between the neighbored fullerene nanodomains is a constant and equivalent to the PDMS chain length on average. Therefore, the increase in the fullerene content can only increase the size of individual fullerene nanodomains. However, in this work, we chose the side chain functionalized PDMS chains to complex with fullerene derivatives. Compared with the terminal funtionalized PDMS chains, there are much more complexing sites available for MPF molecules to bind along the PDMS chains. Thus, the increase in MPF content increases the number of MPF nanodomains in the composites, resulting in a denser packing of fullerene domains. This characteristic structure of PSIXMPF composites leads to a series of special properties of the PDMS–fullerene composite materials.

Fig. 4 shows the typical atomic force microscopy (AFM) topograph images of the composite PSI45MPF15 (A) and PSI45MPF56 (B) films coated on mica surface. The surface morphology of the composite films shows that there are some C_{60} MPF nanodomains being assembled into the PDMS polymer matrix. At low MPF content of 5.2 wt % (A), the dispersion of MPF nanodomains in the PDMS matrix is quite inhomogeneous. When the MPF content is increased to 17.1 wt % (B), the dispersion of the MPF nanodomains becomes more homogeneous. On average, the MPF nanodomains are relatively closer at the higher MPF content. This structure information is consistent with SAXS results. While AFM images only reflect the surface structures of the composite films, transmission electron microscopy (TEM) was also applied to image the structures of the nanocomposites. Fig. 4C shows a typical TEM image of the composite PSI45MPF56 (17.1 wt % MPF) film dried from the solution casting on a copper grid. The TEM image clearly indicates that the self-assembled MPF nanodomains are well dispersed in the PDMS matrix. Due to the random distribution of COOH functional groups along the PDMS chains, the inter-distance of MPF nanodomains has also a broad distribution, which explains the broad scattering peak in the SAXS curves. The size of the MPF nanodomains is about 10 nm.

3.3. Thermal analyses

Fig. 5 shows the DSC traces of PSI45MPF composites at different content of MPF. The PSI45 polymer shows a single T_g at −66 °C. The composites PSI45MPF15 and PSI45MPF36 with low content of MPF also show single T_gs at −64 °C and −66 °C, respectively, indicating the homogeneity of polymer

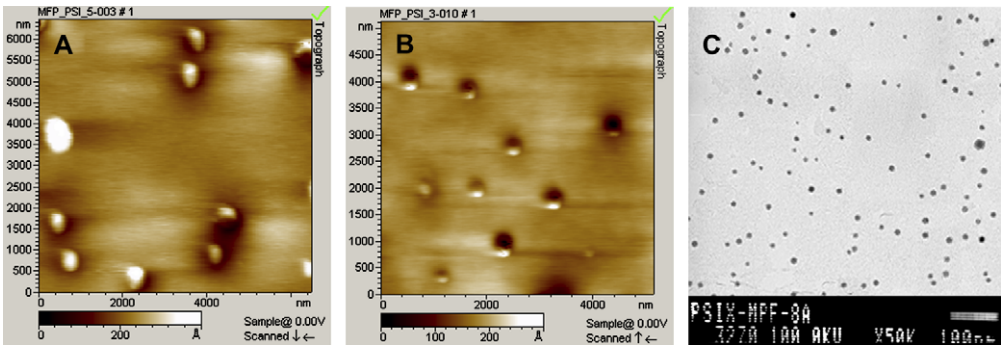

Fig. 4. AFM images of composite films of PSI45MPF15 (A) and PSI45MPF56 (B) and TEM image of composite PSI45MPF56 (C).

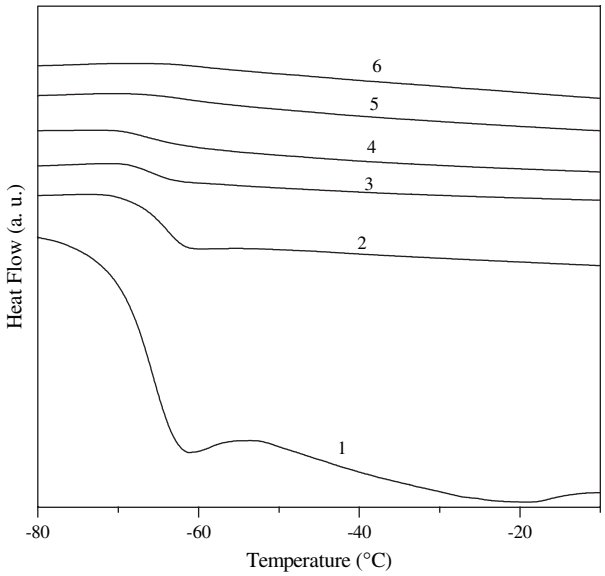

Fig. 5. DSC traces of PSI45MPF composites: (1) PSI45; (2) PSI45MPF15; (3) PSI45MPF36; (4) PSI45MPF56; (5) PSI45MPF74; and (6) PSI45MPF116.

chain segments in terms of flexibility at low content of MPF. The identical T_gs of these two composites with that of PSI45 within the experimental error show that the rigidity of PDMS chain segments caused by low extent crosslinking of MPF nanodomains is just comparable to that by the self-association of carboxylic groups of PSI45. On the other hand, the glass transition broadness of these two composites PSI45MPF15 (12 °C) and PSI45MPF36 (9 °C) becomes much narrower in comparison with that of PSI45 (21 °C), which may be due to the improvement of homogeneity of chain motion after crosslinking with MPF. The inhomogeneity in molecular weight and the extent of functionality of the PDMS matrix, which contribute to the broadness of the glass transition of PSI45, were suppressed by light crosslinking with MPF. However, when the MPF content was increased to certain high level in the PSI45MPF composites (e.g., N/COOH $\geq$ 56 mol %), no distinctive T_gs could be detected due to the rigidity of the highly crosslinked PDMS chains at the high content of MPF nanodomains.

Fig. 6 shows the thermogravimetric traces of PSI45MPF composites. The traces of all composites are in between those of MPF and PSI45, indicating that the thermal stability of PSI45MPF composites makes compromise between their two components. The results are similar with those of MPF/PAA and MPF/PMAA complexes [25] but different from those of fullerenol/end-functionalized PDMS composites [24], where the composites present better thermal stability than their components. This difference could be attributed to the structure difference of the two types of composites as discussed above. PSIX are side-functionalized PDMS, whose thermal degradation process is random depolymerization along the chain, while the end-functionalized PDMS depolymerizes mainly

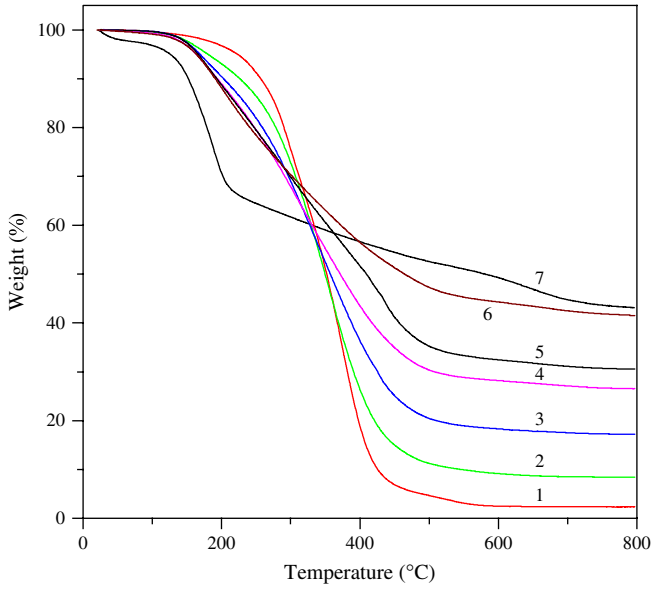

Fig. 6. Thermogravimetric analyses of PSI45MPF composites: (1) PSI45; (2) PSI45MPF15; (3) PSI45MPF36; (4) PSI45MPF56; (5) PSI45MPF74; (6) PSI45MPF116; and (7) MPF.

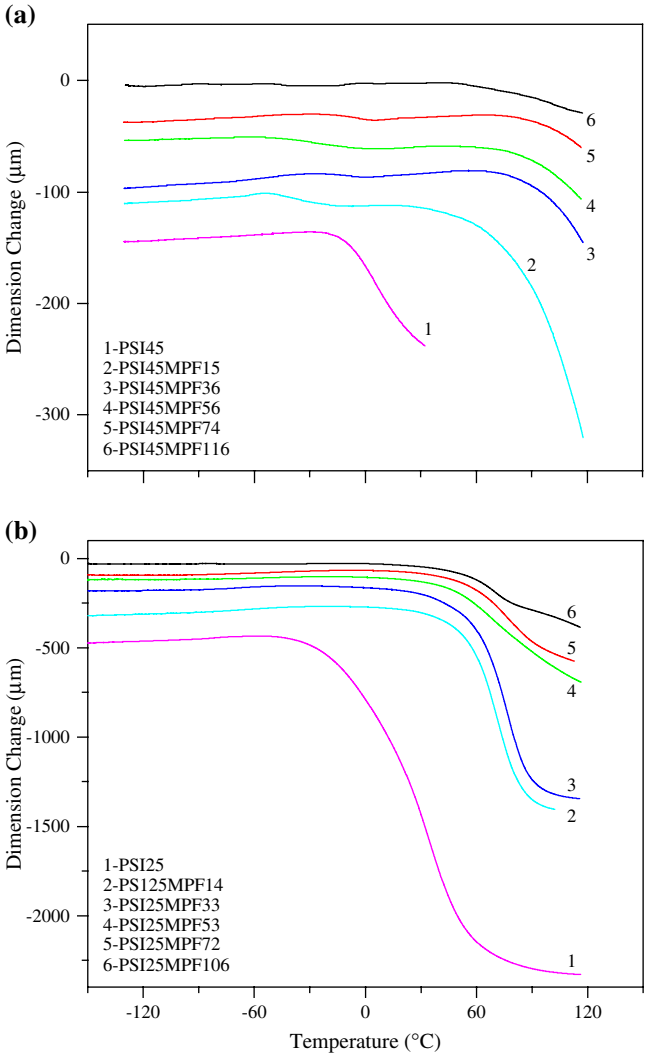

Fig. 7. Thermal mechanical analyses of PSI45MPF composites (a) and PSI25MPF composites (b), respectively. Curves vertically shifted for clarity.

from chain ends [36]. In fullerenol/end-functionalized PDMS composites, the two terminal groups can be effectively anchored with fullerenol molecules, therefore, the composites show improved thermal stability. In PSIXMPF composites, the PDMS matrix is greatly functionalized in the side chains, which are unable to be completely anchored and stabilized by MPF because of the steric hindrance.

Fig. 7a shows the dependence of dimension change with temperature for PSI45MPF composites. PSI45 reveals its softening point at −20 °C, while all the composites show much higher softening temperatures, which increase with the increase in the content of MPF. For instance, the softening temperature of composite PSI45MPF74 is as high as 100 °C. The dramatic increase of softening temperature shows that MPF has significant effects on the thermal mechanical performance of PSI45, which is due to the strong interactions between MPF and PSI45 matrix. It is also observed that there are small softening regions appearing at lower temperatures for composites, with the onsets at −50, −20, −30, −10 °C for composites PSI45MPF15, PSI45MPF36, PSI45MPF56, and PSI45MPF74, respectively. The inner heterogeneity of the composites may account for these softening regions at lower temperatures. The heterogeneity might mainly come from the broad distribution of side functional carboxylic acid groups along the PDMS chains.

Fig. 7b shows the TMA curves of PSI25MPF composites. The softening point of PSI25 locates at −40 °C, which is 20 °C lower than that of PSI45. The lower content of −COOH in PSI25 causes the smaller percentage of self-crosslink, leading to a lower softening temperature. Similarly, the introduction of MPF into PSI25 dramatically increases the softening temperature of PSI25 due to the crosslinking structures. The composites only show single softening points, indicating that inner structures are more homogeneous in PSI25MPF composites than that of PSI45MPF composites.

3.4. Viscoelastic behaviors

Fig. 8 compares storage moduli (G') and loss moduli (G'') of PSI45MPF composites with those of the PSI45 precursor at 1 Hz. The incorporation of MPF into PSI45 dramatically increases both G' and G'' by orders of magnitude, and G' and G'' increase with increasing the content of MPF. A viscous behavior is observed with $G'' > G'$ in the PSI45 sample, while G' exceeds G'' in all the composites, indicating elastic response dominates after complexing of PSI45 with MPF. The viscoelastic property of composites at higher content of MPF (e.g., N/COOH ≥ 74 mol %) cannot be measured by the rheometer of our lab since they are too rigid. It is worthy to mention that the G' platform of PSI45 starting from about 40 °C is the characteristic for crosslinking structures that come from the self-association of carboxylic groups in PSI45. The crosslinking structures begin to rupture from 100 °C as shown by the abruptly decreasing G' value. While milder rupture of the crosslinking structures from ~110 °C is observed for composite PSI45MPF15, the rupture of crosslinking structures disappears in the composites PSI45MPF36 and PSI45MPF56 within the experimental temperature range

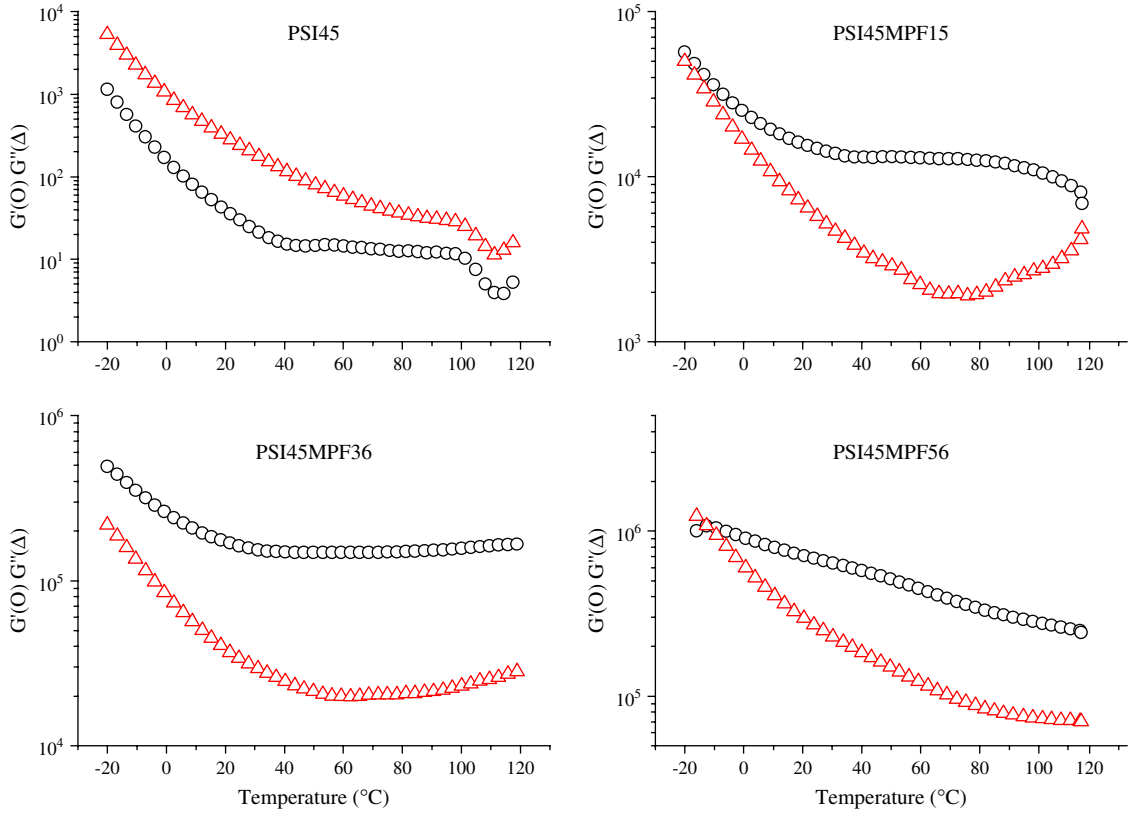

Fig. 8. Temperature dependence of storage moduli G'(○) and loss moduli G''(Δ) of PSI45MPF composites at 1 Hz.

of 120 °C, which may be due to the higher thermal stability of the interactions of MPF with PSI45 as compared to PSI45 self-association. It should be mentioned that the complexing between PSI25 and MPF has similar effects on the viscoelastic behavior of PSI25MPF composites. While PSI25 shows a viscous behavior with $G'' > G'$, all PSI25MPF composites exhibit much higher G' and G'' as well as the elastic behaviors with $G' > G''$. The G' and G'' values also increase with the increase in the content of MPF. However, compared to the PSI45MPF system, the platform of G' curves of PSI25MPF composites starts from ca. 70 °C, which is 30 °C higher than that for PSI45MPF system, indicating a lower crosslinking density in PSI25MPF system due to the lower density of carboxylic groups of PSI25 matrix.

3.5. Dielectric properties

Fig. 9 shows the temperature dependence of dielectric permittivity ε' and loss factor ε'' of PSI45, MPF, and composite PSI45MPF36 at various frequencies. For PSI45, ε' shows a transition with increased ε' value and ε'' shows a relaxation peak from −100 to −64 °C at 1 Hz, corresponding to its glass transition, at which the great increase of chain mobility causes the rapid increase of ε' and ε''. The dynamic glass transition temperature is −79 °C, corresponding to the relaxation peak at 1 Hz. Both ε' transition and ε'' peak become broader and move to high temperatures with increasing frequency. In other words, the relaxation is getting more uniform and homogenized at lower frequency since there is more time to adjust

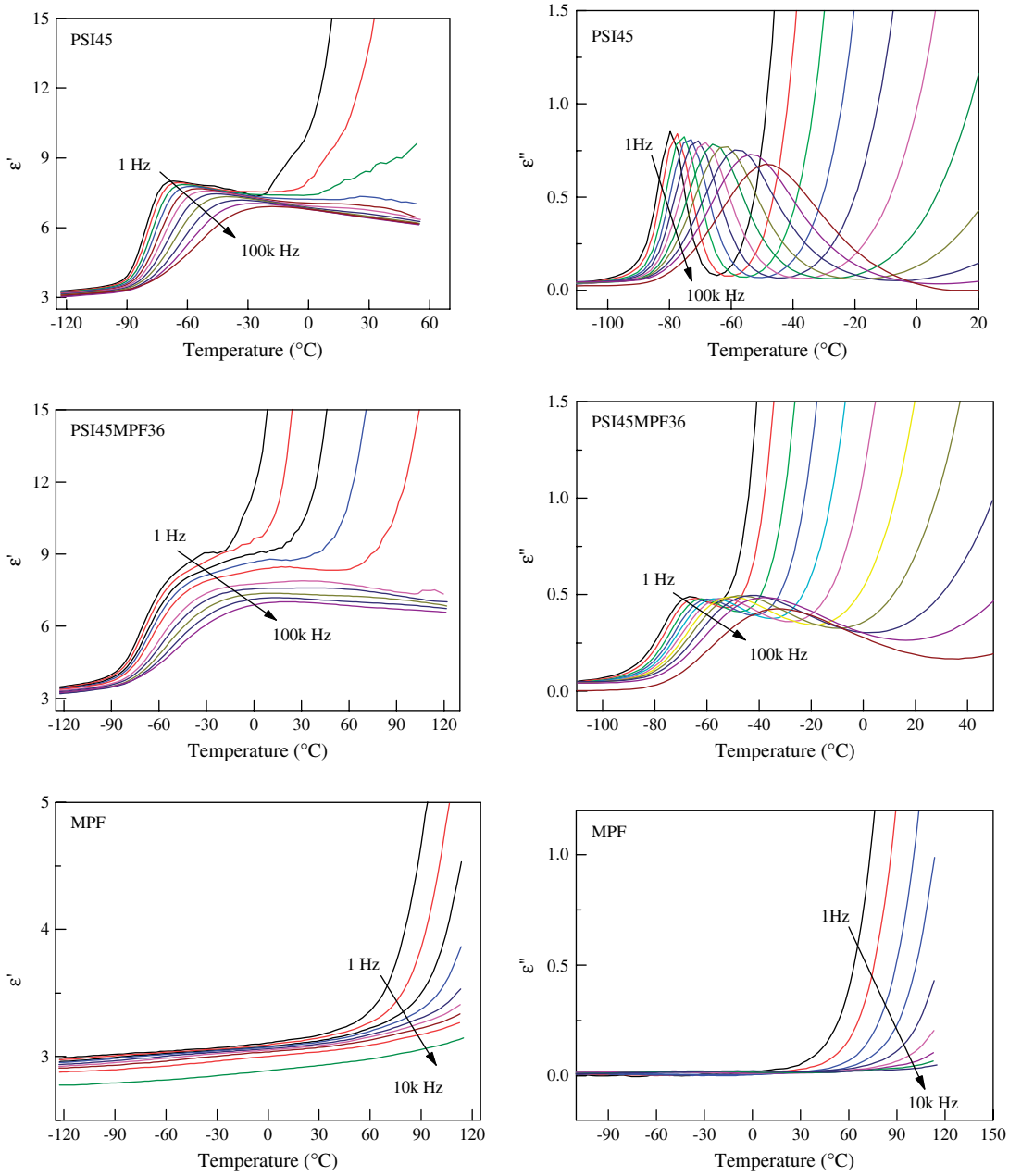

Fig. 9. Temperature dependence of dielectric permittivity ε' and loss factor ε'' at various frequencies for PSI45, PSI45MPF36 composite, and MPF, respectively.

to environmental change. The ε' value of MPF gradually increases with temperature and its ε'' value is near zero. In contrast, the dielectric spectra of composite PSI45MPF36 show a combination of dielectric spectra from the MPF and PDMS components. Compared to PSI45, the composite PSI45MPF36 shows a broader ε' step as well as a broad and squatter ε'' peak, which is due to the addition of MPF nanodomains with much lower ε' and ε'' values and the heterogeneity caused by crosslinking structures. Moreover, the ε'' peak of composite PSI45MPF36 moves to higher temperatures, which is ascribed to the restriction of chain mobility arising from crosslinking. The rapid increases of both ε' and ε'' at high temperature or low frequency for all samples are due to dc conductivity.

4. Conclusions

Supramolecular assembled poly(dimethylsiloxane)/Fullerene nanocomposites could be prepared through the strong ionic interactions of amino groups in MPF and the side carboxylic acid groups on the PDMS chains. SAXS study shows that the MPF nanodomains are homogeneously dispersed in the PDMS matrix without highly ordered close packing structures, which is confirmed with TEM images. The increase in the MPF content leads to a denser packing of fullerene nanodomains in the composites until all COOH functional groups on the PDMS chains were complexed with MPF molecules. This structure change is different from the structures of composites formed by end-functionalized PDMS complexing with multifunctional fullerenes. Compared to its polymeric precursor, the composites exhibit superior thermal mechanical stability. The incorporation of MPF nanodomains into the side carboxylated PDMS matrix dramatically increases the storage and loss moduli of composite materials. The elastic response exceeds viscous response in all the composites due to the formation of crosslinking structures. The higher the MPF content in composites and the carboxylic acid group content on the PDMS chains, the higher the crosslinking density of the composites. Furthermore, the composite shows a combined dielectric property from both the PDMS and MPF components.

Acknowledgements

We acknowledge the financial support for this work from the National Science Foundation (CHE 0316078). S.Z. is grateful to Dr. Igors Scis for his help on the X-ray beamline set up for the SAXS experiments and Mr. Kai Su for his help on the AFM experiments.

References

[1] Jensen AW, Wilson SR, Schuster DI. Bioorg Med Chem 1996;4:767.
[2] Withers JC, Loutfy RO, Lowe TP. Fullerene Sci Technol 1997;5:1.
[3] Imahori H, Sakata Y. Adv Mater 1997;9:537.
[4] Prato M. J Mater Chem 1997;7:1097.
[5] Smalley RE, Yakobson BI. Solid State Commun 1998;107:597.
[6] Sun YP, Riggs JE. Int Rev Phys Chem 1999;18:43.
[7] Diederich F, Gómez-López M. Chem Soc Rev 1999;28:263.
[8] Wudl FJ. Mater Chem 2002;12:1959.
[9] Rincon ME, Hu H, Campos J, Ruiz-Garcia J. J Phys Chem B 2003; 107:4111.
[10] Chen Y, Huang ZE, Cai RF, Yu BC. Eur Polym J 1998;34:137.
[11] Geckeler KE, Samal S. Polym Int 1999;48:743.
[12] Dai L, Mau AWH, Zhang XJ. Mater Chem 1998;8:325.
[13] Sun YP, Lawson GE, Huang W, Wright AD, Moton DK. Macromolecules 1999;32:8747.
[14] Huang XD, Goh SH. Macromolecules 2000;33:8894.
[15] Zhou P, Chen GQ, Hong H, Du FS, Li ZC, Li FM. Macromolecules 2000;33:1948.
[16] He JD, Wang J, Li SD, Cheung MK. J Appl Polym Sci 2001;81:1286.
[17] Ford WT, Lary AL, Mourey TH. Macromolecules 2001;34:5819.
[18] Brabec CJ, Dyakonov V, Sariciftci NS, Graupner W, Leising G, Hummelen JC. J Chem Phys 1998;109:1185.
[19] Lu Z, He C, Chung TS. Polymer 2001;42:5233.
[20] Biswas M, Ray SS. Synth Met 2001;123:135.
[21] Ouyang JY, Goh SH, Li Y. Chem Phys Lett 2001;347:344.
[22] Ouyang JY, Goh SH. Fullerenes Nanotubes Carbon Nanotubes 2002; 10:183.
[23] Ouyang JY, Goh SH, Elim HI, Meng GC, Ji W. Chem Phys Lett 2002;366:224.
[24] Ouyang JY, Zhou SQ, Wang F, Goh SH. J Phys Chem B 2004;108:5937.
[25] Goh SH, Lee SY, Lu ZH, Huan CHA. Macromol Chem Phys 2000; 201:1037.
[26] Clarson SJ, Semlyen JA, editors. Siloxane polymers. NJ: Prentice Hall; 1993. p. 216–44.
[27] Jones RG, Ando W, Chojnowski J, editors. Silicon-containing polymers. The Netherlands: Kluwer Academic Publishers; 2000. p. 185–243.
[28] Li X, Goh SH, Lai YH, Wee ATS. Polymer 2000;41:6563.
[29] Zhou X, Goh SH, Lee SY, Tan KL. Polymer 1998;39:3631.
[30] Landry CJT, Teegarden DM. Macromolecules 1991;24:4310.
[31] Goh SH, Lee SY, Dai J, Tan KL. Polymer 1996;37:5305.
[32] Zhou X, Goh SH, Lee SY, Tan KL. Appl Surf Sci 1998;126:141.
[33] Zhou X, Goh SH, Lee SY, Tan KL. Polymer 1998;39:3631.
[34] Luo XF, Goh SH, Lee SY, Tan KL. Macromolecules 1998;31:3251.
[35] Luo XF, Goh SH, Lee SY, Huan CHA. Macromol Chem Phys 1999; 200:874.
[36] Radhakrishnan TS. J Appl Polym Sci 1999;73:441.